Application of Surface-Based Scale Distributions to Characterize Liquid Sprays: Influence of the Liquid Properties

Christophe Dumouchel, Sébastien Grout, Jean Cousin

ILASS 2008
Sep. 8-10, 2008, Como Lake, Italy

Paper ID ILASS08-A091

APPLICATION OF SURFACE-BASED SCALE DISTRIBUTIONS TO CHARACTERIZE LIQUID SPRAYS: INFLUENCE OF THE LIQUID PROPERTIES

Christophe Dumouchel, Sébastien Grout, Jean Cousin

CNRS UMR 6614 – CORIA
Université et INSA de Rouen
Avenue de l'Université – BP 12
76801 Saint-Etienne du Rouvray, France

ABSTRACT

Recent liquid spray images evidence that in many situations, the droplets are barely spherical. Despite this, it is common to describe the drop-size distribution of spray, which is one of the most important spray characteristic, by attributing a single length scale to each element often defined as an equivalent diameter. In this paper, a new type of 2D liquid spray image description is applied on a series of sprays produced by a single-orifice compound nozzle used with several liquids. This description is called the surface-based scale distribution. Contrary to the previous equivalent-diameter distribution, the surface-based scale distribution and the associated mean scale series are functions of the shape of the droplets. This distribution shows specific properties that are presented in this paper. The application of this new description shows that the surface-based scale is clearly dependent on the liquid properties and on the injection pressure. Among other results, it is found that the first-order mean scale correlates with the injection pressure in a way that, contrary to the traditional mean diameter, is similar from one fluid to another. This behavior is believed to be a characteristic feature of the atomization mechanism. In conclusion, the surface-based scale distribution appears to be an interesting alternative to describe 2D liquid spray images.

INTRODUCTION

The drop-size distribution is one of the most important liquid spray characteristics because the efficiency of any processes involving a spray depends on the size of the liquid elements that constitute the spray. This is why many investigations have been carried out on the development of models to predict this characteristic or of diagnostics to measure it.

From a mathematical point of view, several types of drop-size distribution are defined depending on whether each drop is treated as an event, a length, a surface or a volume [1]. These distributions assume that the droplets are spherical and attribute a diameter to each element. Furthermore, models developed so far to predict spray drop-size distribution are also limited to spherical droplets. (Details on these models are available in [2].)

The experimental diagnostics based on liquid drop light scattering (PDPA, laser diffraction) report a drop-size population distributed on the diameter space [3]. The diameter distribution reported by the PDPA characterizes the drops of the spray that are spherical since this diagnostic can measure spherical droplets only. The liquid elements that don't satisfy this requirement are excluded from the measurement. PDPA drop-size distribution might suffer from incompleteness.

On the other hand, the diameter distribution reported by the laser diffraction technique corresponds to the population of spherical droplets that has the same diffraction pattern as the one recorded. Since the diffraction pattern is a function of the shape of the droplets [4], the distribution provided by the laser diffraction technique is implicitly dependent on this droplet characteristic but this information is hidden.

Techniques based on 2D spray image analysis attribute an equivalent diameter to each element. This diameter is usually defined from the conservation of the projected surface area of each drop [5-7]. However, these approaches clearly evidenced a lack of circularity of the droplets in many situations suggesting that the use of equivalent diameter might not be appropriate.

More recently Dumouchel et al. [8] introduced the surface-based scale distribution to analyze 2D liquid spray images. This distribution and its mean-scale series are explicitly functions of the shape of the liquid elements. The purpose of the investigation reported in this paper is to study the influence of the liquid properties of the surface-based scale distribution and to investigate the advantages and properties of this new way of characterizing liquid spray that is presented in the next section.

THE SURFACE-BASED SCALE DISTRIBUTION

A detailed definition of the surface-based scale distribution is available in Dumouchel et al. [8]. This section summarizes this definition and introduces the main characteristics of this distribution. Let us consider a 2D image containing N objects of any shape as the one illustrated in Fig. 1. Each object on the image is described as follows. We consider the line defined by the inner point located at a given distance r from the boundary of the object (see Fig. 1). For each distance r, called the observation scale, the delimited surface $\mathcal{S}(r)$ (gray surface in Fig. 1) is calculated. When the observation scale covers the whole object, the delimited surface $\mathcal{S}(r)$ is equal to the object total surface area $\mathcal{S}_T$ and the delimited surface $\mathcal{S}(r)$ is kept equal to $\mathcal{S}_T$ for any greater observation scale. For the set of N

objects, the cumulative surface-based scale distribution $S(r)$ is defined by:

$$S(r) = \frac{\sum_{i=1}^{N} \mathcal{S}_i(r)}{\sum_{i=1}^{N} \mathcal{S}_{Ti}} \quad (1)$$

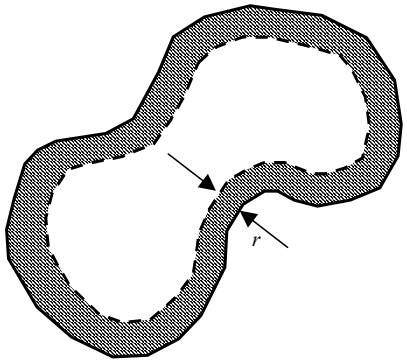

Fig. 1: Description at scale r of an object of any shape

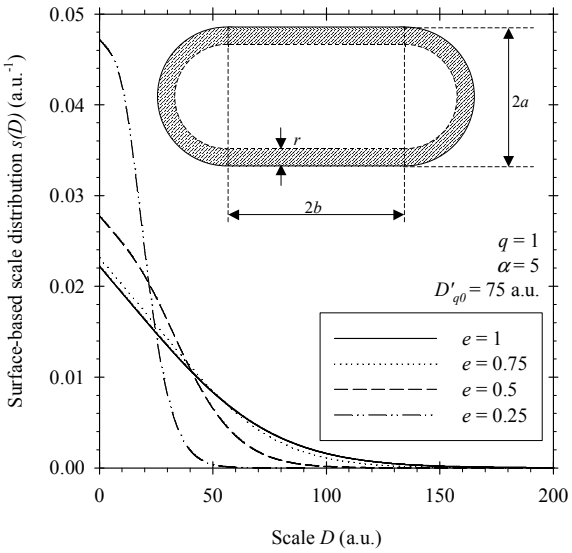

Fig. 2: Definition of a cigar and surface-based scale distribution of sets of cigars with equivalent diameter distributed according to a three-parameter Generalized Gamma distribution. Influence of the shape parameter e.

This cumulative distribution monotonously increases from 0 to 1. As traditionally done for diameter distributions, the first derivative of the cumulative surface-based scale distribution can also be used to characterize the set of objects introducing the function $s(r)$:

$$s(r) = \frac{dS(r)}{dr} \quad (2)$$

that is called the surface-based scale distribution. This function is normalized, i.e., the area delimited by $s(r)$ is equal to 1, namely:

$$\int_0^\infty s(r)dr = 1 \quad (3)$$

In the following, the observation scale r is replaced by $D = 2r$. Thus, the required scale D to fully cover a circular object is equal to its diameter.

The advantage of the surface-based scale distribution is that this description is a function of the shape of the object. To illustrate this we consider sets of elongated objects, called cigars, as the one shown in Fig. 2. A cigar is constituted of a $2a$x$2b$ rectangle ended by two half-circles of radius a. We introduce the equivalent diameter D' defined as the diameter of the circle that has the same surface area as the cigar, namely:

$$D' = \sqrt{\frac{16ab}{\pi} + 4a^2} \quad (4)$$

We introduce the cigar shape parameter e as:

$$e = 2a/D' \quad (5)$$

This parameter is equal to 1 for a circle and decreases towards 0 as the cigar is more and more elongated. We consider a set of cigars with identical shape parameter e but with equivalent diameters D' distributed according to the surface-based diameter distribution given by:

$$f_s(D') = \frac{q}{\Gamma\left(\frac{\alpha+2}{q}\right)} \left(\frac{\alpha}{q}\right)^{\frac{\alpha+2}{q}} \frac{D'^{\alpha+1}}{D'_{q0}{}^{\alpha+2}} exp\left(-\frac{\alpha}{q}\left(\frac{D'}{D'_{q0}}\right)^q\right) \quad (6)$$

where q, α and D'_{q0} are three independent parameters. The number-based diameter distribution associated to the surface-based distribution given by Eq. (6) is a three-parameter Generalized Gamma function that is identical to the well-known Nukiyama-Tanasawa distribution (Dumouchel [9]). The surface-based scale distribution can be expressed as a function of the shape parameter e and the distribution $f_s(D')$ (see Dumouchel et al. [8] for details). Figure 2 shows the surface-based scale distributions of four sets of cigars: the sets have the same surface-based equivalent diameter distribution ($q = 1$, $\alpha = 5$, $D'_{q0} = 75$ a.u.) but differ by the shape parameter e of the objects they contain. It can be seen that contrary to the traditional diameter distribution, the surface-based scale distribution is a monotonously decreasing function. Furthermore, this function is clearly dependent on the shape of the objects. In Fig. 2, the case $e = 1$ correspond to circular objects. When e decreases, the objects are more and more elongated whereas the total surface area is kept constant. Thus, when e decreases, the proportion of surface recovered at small observation scale increases since the total interface length increases, and the greatest observation scale to cover all the objects decreases. This explains why, when e decreases, the maximum $s(D)$ increases and the greatest scale decreases.

It can be also noticed in Fig. 2 that when the observation scale approaches zero, $s(D)$ adopts a linear behavior with a slope that is independent of the parameter e. Dumouchel et al. [8] showed that as long as the observation scale is smaller than the scale that fully recover the smallest element, the surface-based scale distribution is linear. Furthermore, whatever the

situation, the slope of this linear portion of the surface-based scale distribution *s(D)* is given by:

$$s'(0) = -\frac{2}{D'^{2}_{20}} \tag{7}$$

where D'_{20} is a mean diameter of the surface-based equivalent diameter distribution belonging to the mean diameter series standardized by Mugele and Evans [10]. For the four cigar sets shown in Fig. 2, this mean diameter is the same because the equivalent diameters are distributed according to the same surface-based function explaining why the surface-based scale distributions are parallel to each other when the observation scale approaches zero.

As done for the diameter distribution description, it is possible to define a series of mean scale Ds_n by the relation:

$$(Ds_n)^n = \int_0^\infty s(D) D^n dD \tag{8}$$

For a set of cigars, Dumouchel et al. [8] demonstrated that this mean scale series could be expressed as a function of the mean equivalent diameter series and of the shape parameter, namely:

$$(Ds_n)^n = (eD'_{n+2,2})^n \left(\frac{2 + n(1 - e^2)}{(n+1)(n+2)} \right) \tag{9}$$

For a set of circular objects ($e = 1$), Eq. (9) indicates that $Ds_1 = D'_{32}/3$, where D'_{32} is the Sauter mean diameter of the equivalent diameter distribution. In other words, the ratio $3Ds_1/D'_{32}$ can be seen as a mean shape parameter of the all set: when this ratio is equal to 1, the set is composed of circular objects, otherwise, the ratio is less than 1. Furthermore, the ratio is less and less as the objects are more and more deformed.

EXPERIMENTAL SETUP AND DIAGNOSTIC

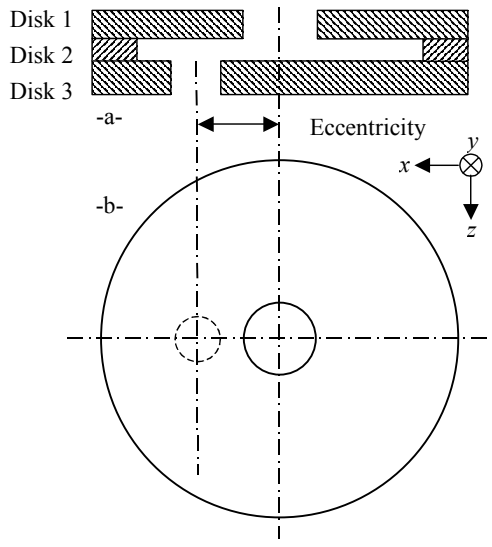

Fig. 3: Simplified compound nozzle

The experimental set-up is summarized only because details can be found elsewhere [11]. A simplified compound nozzle (Fig. 3) having a unique discharge orifice with a diameter equal to 180 µm produces the spray. This nozzle was inspired from compound nozzle encountered in low-pressure port-fuel injection engines. The nozzle internal geometry imposes drastic flow deflections and favors the development of a double-swirl at the nozzle exit as well as a consistent turbulent level. As soon as the liquid issues from the nozzle, the double-swirl induces a radial expansion of the jet and modifies it as a sheet. The turbulence imposes perturbations on the liquid-gas interface that favor an early disintegration process. A previous study conducted on these atomizers showed that the total energy E_T available for atomization is the sum of two kinetic energies calculated at the nozzle exit, namely, the non-axial flow component kinetic energy (that characterizes the double–swirl structure) and the turbulent kinetic energy (Dumouchel et al. [13]). It was found that the spray surface energy per unit liquid volume σ/D'_{32} (where D'_{32} is the spray Sauter mean diameter) is linearly dependent on the energy E_T. In that study, the Sauter mean diameter was measured with a diffraction technique and the total energy available for atomization was evaluated at the nozzle exit from calculations of the internal flow conducted with the code Fluent. The linear relationship between σ/D'_{32} and E_T was found to be independent of the nozzle geometry and is believed to be a characteristic feature of the atomization process promoted by this kind of injector.

Shadowgraph images of the flow issuing from the nozzle are taken with a high-resolution camera (2016x3040 pixel^2) and a short light source (11 ns). The image covers a field of 10.5x7 mm^2 with a spatial resolution equal to 3.47 µm/pixel. The analyzed drops are within a window that is 600 pixels in height and as large as the image (2016 pixels). This window is positioned at the bottom of the image. The drops are detected on the green frame of the images since its 256 gray-level distribution allows the droplets to be best dissociated from the background. In each image, this distribution reported two peaks, one being representative of the droplets and the other one to the background. A gray-level threshold is calculated from the mode and the standard deviation of the gray-level histogram. Pixels with a gray-level greater than the threshold are identified as background pixels. If not, they are identified as liquid pixels. However, the background peak position considerably differs from one image to another. Therefore, the gray-level threshold to dissociate droplets from the background and to create the two gray-level images is determined on each image.

Before applying the scale distribution analyzing procedure described in the previous section, several tests are performed on each droplet. First, all droplets in contact with the borders of the analyzing window are removed. Second, groups of pixels less than 6 pixels are removed. Thus, the minimum detectable drop diameter is fairly less than 10 µm. Third, light scattered by the drops may have two undesirable effects. On big drops, some internal pixels might have been identified as background pixels. These pixels are easily identifiable and given the liquid gray-level value. Furthermore, some small droplets might be badly encoded and might produce separated groups of pixels due to light scattering. These groups of pixels are characterized by a small equivalent diameter D' (calculated on the surface conservation) and a low circularity parameter C defined as 4π multiplied by the ratio of the surface area to the square of the perimeter. This circularity varies from 0 to 1, the latter value corresponding to a perfect circularity. Because the surface tension cohesion forces are inversely proportional to the drop diameter, small liquid

droplets are expected to be spherical and characterized by rather high circularity C. After several tests, we obtained a condition to identify non-circular small objects that corresponded to badly encoded droplets: all groups of pixels such that $D' < 75 - 60C$ (where D' is expressed in μm) were removed.

Contrary to the previous investigation that considered a single liquid [13], six different liquids are used in the present investigation. Their physical properties are given in Table 1. The injection pressure ΔP_i was varied according to the liquid in order to insure that the detection in the small-scale range is accurate enough. Thus, for heptane, ΔP_i did not exceed 0.2 MPa. For the other liquids, the maximum injection pressure was 0.5 MPa. The injection pressure limit is smaller for heptane because the surface tension of heptane is smaller and its propensity to create small drops is greater. Furthermore, the two water/glycerol mixtures were used at two injection pressures only, namely, 0.35 and 0.50 MPa. Injections are performed under atmospheric pressure. For each operating condition, 150 images are analyzed. The number of analyzed droplets was a function of the working conditions. It ranged between 3000 and 32000.

Table 1: Liquid physical properties (Wat/Gly.: Water-Glycerol, Wat/Eth.: Water-Ethanol, percentages indicate weight proportion)

Fluid	ρ_L (kgm^{-3})	σ (mNm^{-1})	μ_L (kgm^{-1}s^{-1})
Heptane	704	20.6	$0.41\ 10^{-3}$
Water	991	72.0	$1.00\ 10^{-3}$
Wat/Gly. 5%	1012	70.4	$1.33\ 10^{-3}$
Wat/Gly. 10%	1030	70.2	$1.43\ 10^{-3}$
Wat/Eth. 1%	986	65.9	$1.00\ 10^{-3}$
Wat/Eth. 10%	972	46.1	$1.40\ 10^{-3}$

The surface-based scale distribution is measured by applying the Euclidean Distance Mapping (EDM) method often applied to calculate the fractal dimension of contours (Grout et al. [11]). In the present study, EDM is applied inside the object only. Each internal pixel is allocated a gray level that is equal to the shortest distance, expressed in pixels, between this pixel and the contour of the object. Then, counting the pixels with a gray level less or equal to a given value returns the surface covered at a given observation scale r (see Fig. 1). When all objects are fully covered, the surface becomes independent of the gray level: this surface is equal to the total surface and is used to calculate the cumulative surface-based scale distribution (Eq. (1)) as well as the corresponding surface-based scale distribution using Eq. (2).

The equivalent diameter D' of each object was also measured in order to determine the surface-based equivalent diameter distribution $f_s(D')$ and the corresponding mean diameter series D'_{mn}.

The determination of the surface-based scale distribution $s(D)$ doesn't allow the value of the function at $D = 0$ to be determined: $s(D)$ being the derivative of the cumulative distribution $S(D)$, the smallest scale at which $s(D)$ is obtained corresponds to $r = 2$ pixels, i.e., $D = 4$ pixels. This limitation affects the determination of the mean scale series since the distribution $s(D)$ is maximum in the small scale range. To avoid this problem, the distribution $s(D)$ must be extended to the scale space origin. As a first approximation, this can be achieved by using the fact that the slope of $s(D)$ at $D = 0$ is equal to $-2/D'^2_{20}$ whatever the situation and to impose this slope to the range of scales uncovered by the image analyzing technique. The reliability of this extension procedure is controlled by checking the normalization of the distribution $s(D)$.

RESULTS

Figure 4 shows the surface-based equivalent diameter distribution $f_s(D')$ obtained for the Water/Ethanol 10% liquid as a function of the injection pressure. We note that the evolution of this distribution with the injection pressure is the one expected: when ΔP_i increases the distribution becomes narrower, the peak is greater and is shifted towards the small drop population. Similar results were obtained for other liquids. It is therefore believed that the number of droplets analyzed for each operating condition is sufficient to be statistically representative. As explained by Dumouchel et al. [13] the production of a finer spray when the injection pressure increases is not due to the influence of aerodynamic effects. Indeed, the typical gaseous Weber numbers encountered in these experiments and based on the surrounding gas density and the average issuing flow velocity doesn't not exceed 6 which is too small to expect any assistance of aerodynamic effects on the atomization process. The production of finer sprays when the injection pressure increases is the consequence of an increase of the total energy E_T introduced in the previous section.

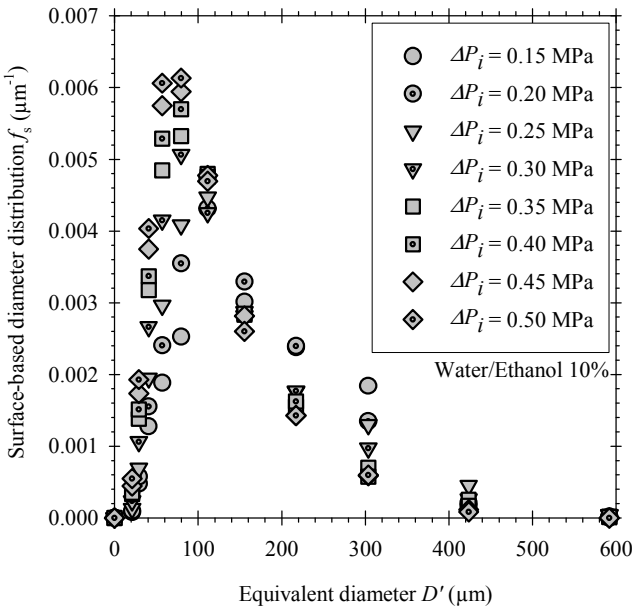

Fig. 4: Surface-based equivalent diameter distribution (Water/Ethanol 10%, Influence of the injection pressure).

The first-order moment of surface-based diameter distribution $f_s(D')$ is the Sauter mean diameter D'_{32} [14]. For each fluid, this mean diameter is shown as a function the injection pressure in Fig. 5. This figure shows that the dependence between the Sauter mean diameter and the injection pressure is a function of the liquid physical properties, the sharpest mean diameter decrease with the injection pressure being obtained for heptane, which is the fluid with the smallest dynamic viscosity and surface tension. As said in the previous section, one of the characteristic features of the atomization mechanism of the flow issuing from the simplified compound nozzle is the linear dependence

between the total energy available for atomization E_T of the issuing flow and the spray surface energy per unit liquid volume σ/D'_{32}. In the present work, the energy E_T was evaluated for all operating conditions following the procedure used by Dumouchel et al. [13]. (This procedure that made use of the numerical simulation code Fluent is described in [13] and is not reported in the present paper.) The ratio σ/D'_{32} as a function of the total energy E_T is shown in Fig. 6. Despite the fact that in the present work the mean equivalent diameters D'_{32} haven't been measured by a laser diffraction technique, a linear dependence between E_T and σ/D'_{32} has been retrieved for each fluid in agreement with Dumouchel et al. [13]. We believe that this result indicates that the atomization mechanism is the same for all operating conditions and is dominated by the double-swirl flow and the turbulence of the issuing liquid flow and by the action of surface tension forces. It is interesting to note here that, whereas Dumouchel et al. [13] found that the relationship between E_T and the ratio σ/D'_{32} was independent of the nozzle dimensions, it is found here that this relationship is a function of the liquid properties.

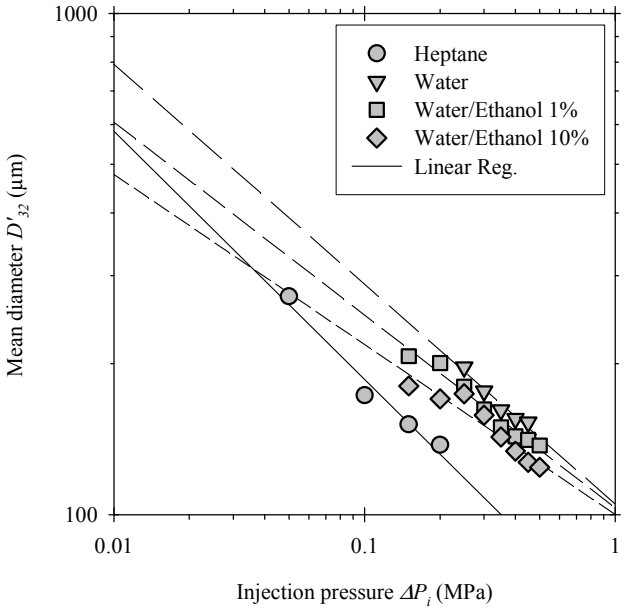

Fig. 5: Mean diameter D'_{32} as a function of the injection pressure (several liquids).

The main objective of this work consists in determining the surface-based scale distribution *s(D)* introduced above for all operating conditions. As explained earlier, it is important to be able to determine this distribution when the observation scale approaches zero since the distribution is maximum at this point. The smallest observation scale that is reachable by the image analyzing technique is equal to 1 pixel, which corresponds to an observation scale $D = 6.94$ µm. To fill the gap between this scale and 0, we make use of Eq. (7): the distribution is extended to $D = 0$ assuming a linear behavior between 0 and 6.94 with a slope given by Eq. (7). The mean diameter D'_{20} in Eq. (7) is derived from the surface-based equivalent diameter distribution $f_s(D')$ as those shown in Fig. 4. These diameters are shown in Fig. 7 for several liquids as a function of the injection pressure. Note that, as observed for the mean equivalent diameter D'_{32} (Fig. 5), the mean equivalent diameters D'_{20} report a clear dependence with the injection pressure, this dependence being a function of the liquid properties. The quality of the extension procedure of the distribution *s(D)* can be evaluated by checking the normalization property, i.e., Eq. (3) must be satisfied. For all cases reported in this paper, the integral given by Eq. (3) was calculated. It was found to range from 0.981 to 0.992, which represents an error less than 1.9%. This result is good enough to validate the extension procedure.

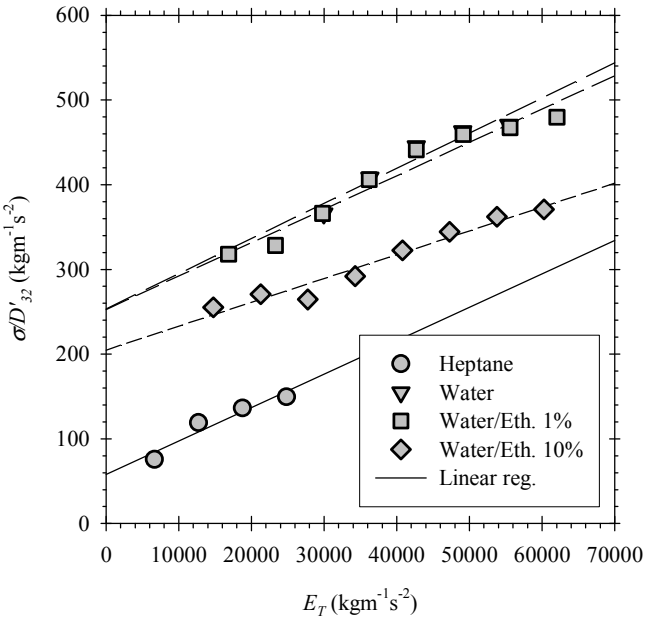

Fig. 6: Evolution of the spray surface energy per unit volume with the energy available for atomization (several liquids and injection pressures).

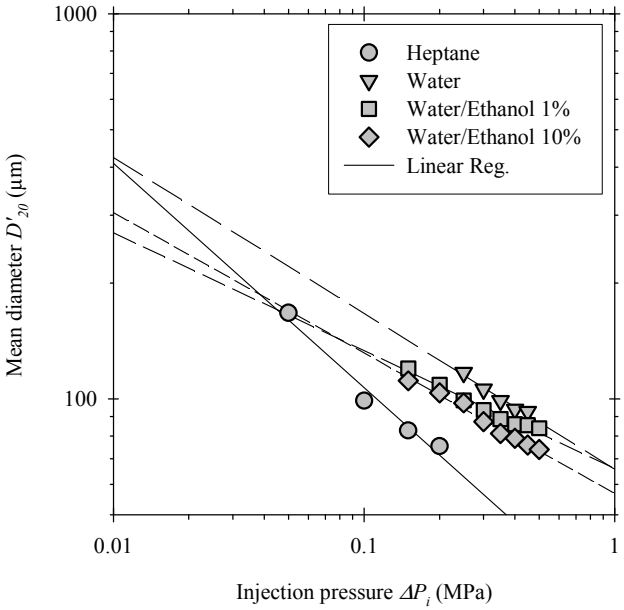

Fig. 7: Mean diameter D'_{20} as a function of the injection pressure (several liquids).

Examples of surface-based scale distributions are presented in Figs. 8 and 9. Figure 8 presents a series of *s(D)* distributions as a function of the injection pressure (Water/Eth. 10%) and Fig. 9 shows a series of distributions as a function of the liquid for a constant injection pressure ($\Delta P_i = 0.35$ MPa). These figures show that the surface-based scale distribution is clearly influenced by both the injection

pressure and the liquid properties. When the injection pressure increases, the maximum scale decreases and consequently the peak at $D = 0$ increases. These behaviors evidence the increase of liquid gas interface length per unit liquid surface area, which is due to the production of smaller or more deformed droplets or to a combination of these two effects.

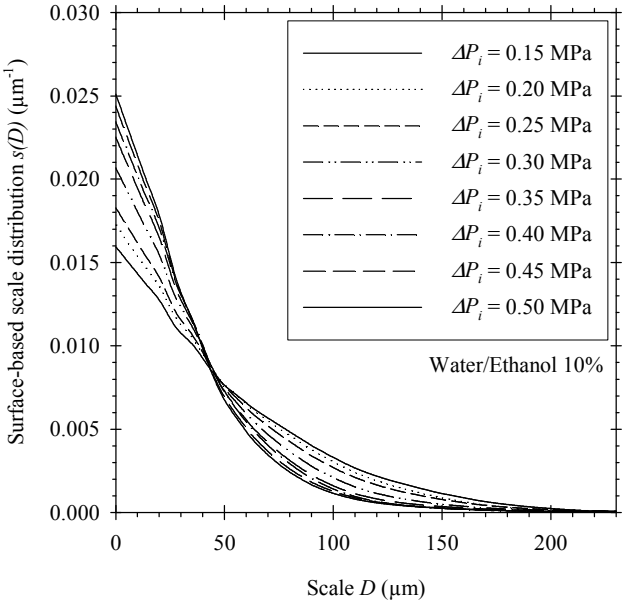

Fig. 8: Surface-based scale distributions *s(D)* (Water/Ethanol, influence of the injection pressure).

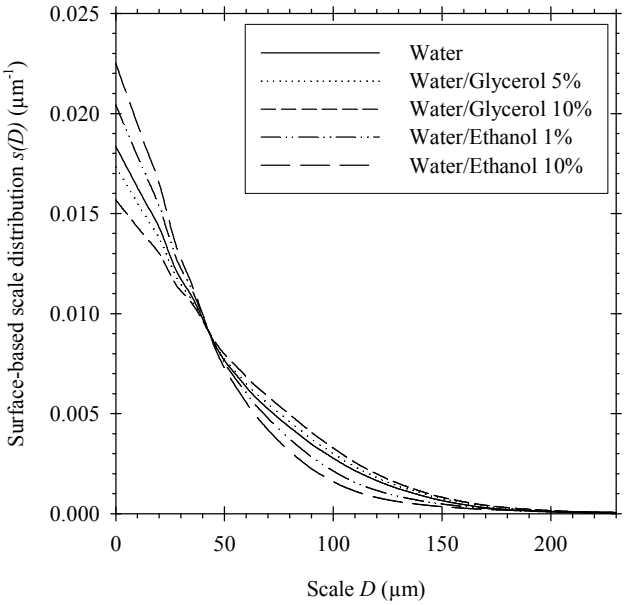

Fig. 9: Surface-based scale distributions *s(D)* (ΔP_i = 0.35 MPa, several liquids).

The results presented in Fig. 9 show that the most viscous fluids (Water/Glycerol mixtures) produce sprays with larger surface-based scale distributions. To the contrary, the fluids with smallest surface tension (Water/Ethanol mixtures) produce sprays with narrower surface-based scale distributions. These observations are the expected ones since as explained above, the level of turbulence in the liquid flow issuing from the nozzle and surface tension forces dominate the atomization mechanism that takes place on the liquid jet produced by the compound atomizer used here. An increase of the liquid viscosity plays against the production of turbulence and consequently reduces the propensity of creating liquid structures with small characteristic scales. Similarly, the increase of surface tension plays against the growth of small perturbations and favors the production of liquid structures with larger characteristic scales. These influences of the liquid properties on the surface-based scale distribution correspond to those reported by Fig. 9.

It is interesting to compare the surface-based diameter distributions presented in Fig 4 with the surface-based scale distributions obtained for the same operating conditions and reported in Fig. 8. Note that, for each operating condition, the maximum equivalent diameter is always much greater than the maximum scale. This illustrates the fact that the greater elements of the spray are not circular. As explained above, considering the ratio $3Ds_1/D'_{32}$ can emphasize this point.

The ratio $3Ds_1/D'_{32}$ allows the lack of circularity of the drops to be evaluated. To determine this ratio, we first calculate the first order moment Ds_1 of the surface-based scale distribution. Using Eq. (8), this moment is given by:

$$Ds_1 = \int_0^\infty s(D) D dD \tag{10}$$

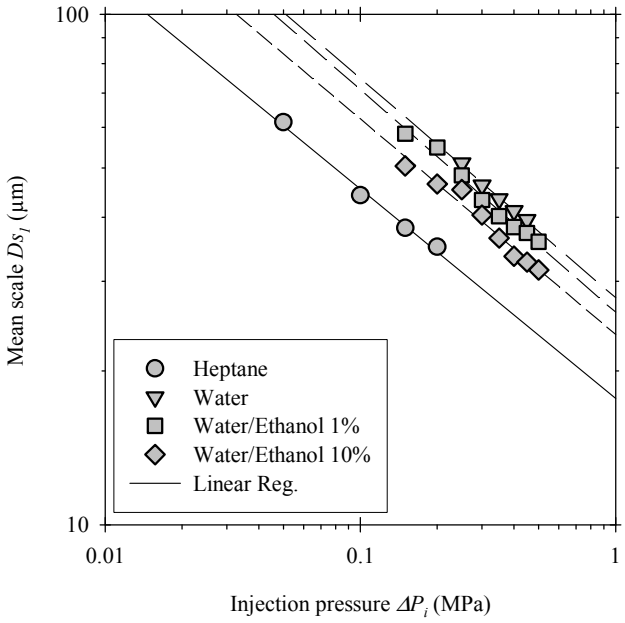

Fig. 10: Evolution of the mean scale Ds_1 as a function of the injection pressure (several fluids).

Figure 10 presents the evolution of the mean scale Ds_1 as a function of the injection pressure for several liquids. The first thing to be noted is that for each liquid, this mean scale strongly correlates with the injection pressure. Furthermore, by comparing Figs. 5 and 7 with Fig. 10 it is interesting to note that, contrary to the traditional mean diameters, the dependence between the injection pressure and the arithmetic mean scale Ds_1 is similar from one fluid to another. The behaviors shown in Fig. 10 report the following relationship between Ds_1 and ΔP_i:

$$Ds_1 = B\Delta P_i^{-0.42} \tag{11}$$

It is instructive to investigate the evolution of the parameter B introduced in Eq. (11) as a function of the liquid physical properties. We found that this parameter is mainly a function of the liquid surface tension. This is illustrated in Fig. 11 that shows the parameter B as a function of the surface tension coefficient for the four liquids considered in Fig. 10. Figure 11 emphasizes a strong linear relationship between the parameter B and the surface tension coefficient. This result suggests that the liquid viscosity has a reduced influence in the relationship between the mean scale Ds_1 and the injection pressure. This conclusion is rather surprising since the liquid viscosity controls the production of turbulence of the liquid flow issuing from the nozzle and that this level of turbulence has been demonstrated to be of paramount importance in the present atomization mechanism. It is believed that the independence between the liquid viscosity and the parameter B reported by Fig. 11 is due to the fact that for the four liquids considered in Figs. 10 and 11, the spray formation is more influenced by the variation of the surface tension than by the variation of the liquid viscosity. Further experimental work should be conducted to confirm this point.

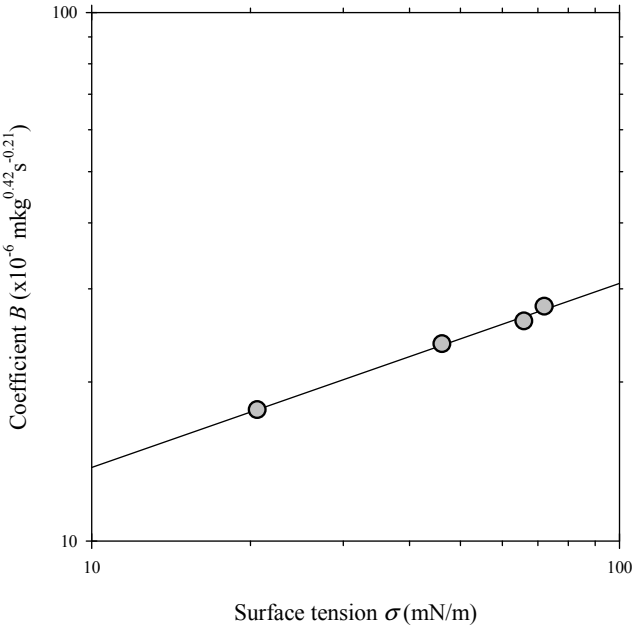

Fig. 11: Relationship between the parameter B (Eq. (11)) and the surface tension coefficient (Heptane, Water and Water/Ethanol mixtures).

Finally, Fig. 12 presents the evolution of the ratio $3Ds_1/D'_{32}$ as a function of the injection pressure for all fluids. As explained above, this parameter can be seen as a shape parameter of the global spray: it is equal to 1 when all droplets delimit circular objects on the image and it is less than 1 otherwise. For all operating conditions examined in this work, we see that this shape parameter varies from 0.68 to 0.84 according to the injection pressure and the liquid. The smallest shape parameters are obtained when the injection pressure is low (heptane at 0.05 MPa) and for the liquid that has the highest viscosity (Water/Glycerol 10% at 0.35 MPa). In both cases, the turbulent level of the issuing flow is believed to be too low to promote liquid structures with small characteristic scales. On another hand, the liquid structures produced in these conditions have a less propensity to become spherical. As the injection pressure increases it can be seen that the shape parameter seems to evolve towards an asymptotic value that slightly depends on the liquid physical properties. This value is believed to be a characteristic of the atomization mechanism.

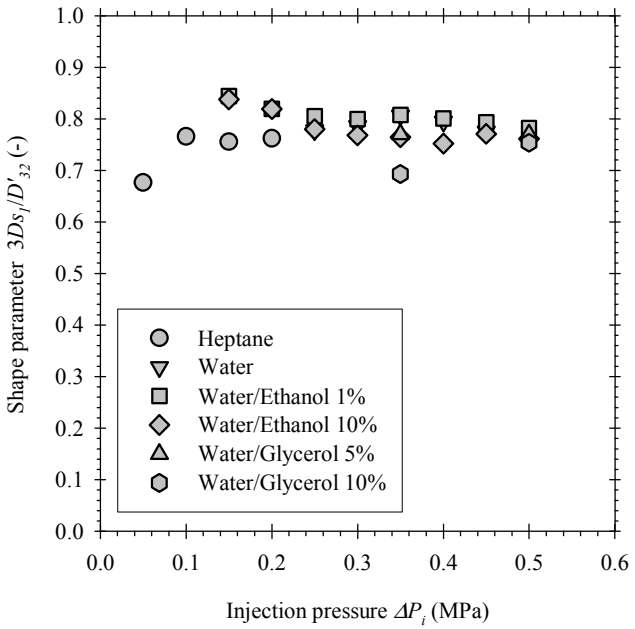

Fig. 12: Relationship between the ratio $3Ds_1/D'_{32}$ and the injection pressure (all fluids).

CONCLUSIONS

The surface-based scale distribution applied in this paper to several operating conditions appears as an interesting alternative to describe 2D images of liquid spray drops. As noticed by Dumouchel et al. [8], this new description is best adapted to represent sets of objects of identical shape and size. Although this case represents a limited interest, it can be reminded that, for such sets, the traditional diameter distributions are Dirac functions and are unpractical. Furthermore, the surface-based scale distribution is a function of the shape of the objects even if the projected surface area of each object is unchanged. For such situations, the traditional surface-based equivalent-diameter distribution report identical functions whatever the shape of the drops. Thus, the surface-based scale distribution offers a more descriptive characterization.

Contrary to the traditional drop diameter distribution, the surface-based scale distribution (first derivative of the cumulative scale distribution) is a continuously decreasing function. In consequence this distribution is maximum when the observation scale is equal to zero. Furthermore, it presents the following characteristic feature: the distribution shows a linear decrease when the observation scale varies from 0 to the scale that fully covers the smallest characteristic length scale of the whole object set. This latter scale can be either the diameter of the smallest circular object or the diameter of the thinnest ligament. Whatever the situation, the slope of the surface-based distribution in this scale interval is inversely proportional to the square of the mean equivalent-diameter D'_{20}, the equivalent-diameter of each object being defined as the diameter of the circular object that conserves the surface area of the object.

In the present work, the surface-based scale distribution is used to describe spray produced by a single-orifice compound

nozzle but with several liquids. Considering a previous investigation, it is first demonstrated that the atomization mechanism that gives birth to the spray is the same whatever the liquid, namely, the liquid jet issuing from the nozzle is deformed thanks to the presence of a double-swirl flow component as well as of a non-negligible turbulent level. Then, surface tension forces mainly control the evolution of the jet shape and the breakup during the atomization process since the aerodynamic effects have been found to be negligible.

An image analyzing procedure has been developed to measure the surface-based scale distributions as a function of the liquid properties and of the injection pressure. This measurement is satisfactorily extended towards the scale space origin by using the property of the distribution in the small-scale range. To achieve this, the surface-based equivalent-diameter distribution is also measured. It is found that the surface-based scale distribution shows a clear dependence with the injection pressure and with the liquid physical properties. Furthermore, although the mean equivalent-diameters show a correlation with the injection pressure that is a function of the liquid physical properties, it is found that the first-order mean scale shows also a clear correlation with the injection pressure but this correlation appears to be similar from one fluid to another. This behavior is believed to be a characteristic of the atomization mechanism. Experiments conducted for other atomization mechanisms should be conducted to confirm this point. It can be concluded here that the surface-based scale distribution opens new ways of analyzing 2D liquid spray images all the more so since such a description can also be applied on liquid jet during the atomization mechanism. This latter point is currently investigated.

NOMENCLATURE

Symbol	Quantity	SI Unit
a, b	Cigar geometrical characteristics	µm
B	Coefficient introduced in Eq. (11)	$mkg^{0.42}s^{-0.21}$
D	Observation scale (= $2r$)	µm
Ds_n	Mean scale series	µm
D'	Equivalent diameter	µm
D'_{mn}	Mean equivalent diameter series	µm
e	Cigar shape parameter	-
E_T	Available energy for atomization	$kgm^{-1}s^{-2}$
$f_s(D')$	Surface-based equivalent diameter distribution	μm^{-1}
i	Object index	-
N	Number of objects	-
q	Parameter of the surface-based diameter distribution given by Eq. (6)	-
r	Observation scale	µm
$s(r); s(D)$	Surface-based scale distribution	μm^{-1}
$\mathcal{S}(r)$	Surface covered at scale r	μm^2
S_T	Object total surface area	μm^2
$S(r), S(D)$	Cumulative surface-based scale distribution	-
α	Parameter of the surface-based diameter distribution given by Eq. (6)	-
ΔP_i	Injection pressure	MPa
ρ_L	Liquid density	kgm^{-3}
σ	Liquid surface tension	mNm^{-1}
μ_L	Liquid dynamic viscosity	$kgm^{-1}s^{-1}$

REFERENCES

[1] T. Paloposki, Drop-Size Distribution in Liquid Sprays, Ph.D. Thesis, Acta Polytechnica Scandinavica, Mechanical Engineering Series No. 114, Helsinki (1994)

[2] E. Babinski and P.E. Sojka, Modeling Drop-Size Distribution, *Progr. Energy Combust. Sci.*, vol. 28, pp. 303-329 (2002)

[3] L.G. Dodge, D.J. Rhodes and R.D. Reitz, Drop-Size Measurement Techniques for Sprays: Comparison of Malvern Laser-Diffraction and Aerometrics Phase-Doppler, *Applied Optics*, vol. 26, pp. 2144-2154 (1987)

[4] A. Borovoi, E. Naats, U. Oppel and I. Gr-shin, Shape Characterization of a Large Nonspherical Particle by Use of its Fraunhofer Diffraction Pattern, *Applied Optics*, vol. 39, pp. 1989-1997 (2000)

[5] H. Malot and C. Dumouchel, Experimental Investigation of the Drop-Size Distribution of Sprays Produced by a Low-Velocity Newtonian Cylindrical Jet, *Atom. and Sprays*, vol. 11, pp. 227-254 (2001)

[6] Y.D. Kim and S.Y. Lee, Application of Hough Transform to Image Processing of Heavily Overlapped Particles with Spherical Shapes, *Atom. and Sprays*, vol. 12, pp. 451-461 (2002)

[7] J.B. Blaisot and J. Yon, Droplet Size and Morphology Characterization for Dense Sprays by Image Processing: Application to the Diesel Spray, *Exp. in Fluids*, vol. 39, pp. 977-994 (2005)

[8] C. Dumouchel, J. Cousin and S. Grout, Analysis of Two-Dimensional Liquid Spray Images: The Surface-Based Scale Distribution, *Journ. Flow Visua. Image Proc.*, vol. 15, pp. 59-83 (2008)

[9] C. Dumouchel, A New Formulation of the Maximum Entropy Formalism to Model Liquid Spray Drop-Size Distribution, *Part. Part. Syst. Charact.*, vol. 23, pp. 468-479 (2006)

[10] R.A. Mugele and H.D. Evans, Droplet Size Distribution in Sprays, *Ind. Engng. Chem.*, vol. 43, pp. 1317-1324 (1951)

[11] S. Grout, C. Dumouchel, J. Cousin and H. Nuglisch, Fractal Analysis of Atomizing Liquid Flows, *Int. J. Multiphase Flows*, vol. 33, pp. 1023-1044 (2007)

[13] C. Dumouchel, J. Cousin and K. Triballier, On the Role of the Liquid Flow Characteristics on Low-Weber Atomization Processes, *Exp. in Fluids*, vol. 38, pp. 637-647 (2005)

[14] W.A. Sowa, Interpreting Mean Drop Diameters Using Distribution Moments, *Atom. and Sprays*, vol. 2, pp. 1-15 (1992)